# $K$-vacancy production in heavy-ion collisions. IV. $K$-$L$ level matching

W. E. Meyerhof and R. Anholt
*Department of Physics, Stanford University, Stanford, California 94305*

J. Eichler† and A. Salop
*Molecular Physics Center, SRI International, Menlo Park, California 94025*

(Received 27 June 1977)

As shown in papers I and II of this series, far from symmetry the $K$-vacancy production cross section of the lower-$Z$ ($Z_L$) partner in heavy-ion collisions varies rapidly with the atomic number $Z_H$ of the higher-$Z$ partner. We examine our and other data for $K$ and $L$ x-ray production with 45–94-MeV Ni, 45–110-MeV Br, 47- and 62-MeV I projectiles and interpret the $Z_L$ $K$-vacancy production far from symmetry in terms of the $K$-$L$ level matching mechanism of Barat and Lichten. Sharing of $3d\sigma$ vacancies on the outgoing part of the collision provides a semiquantitative understanding of the dependence of $K$ and $L$ cross sections on $Z_L$, $Z_H$, and bombarding energy. Some remarks about the general role of vacancy sharing in inner-shell vacancy formation in heavy-ion collisions are made.

## I. INTRODUCTION

The first papers[1-3] in this series, henceforth called I, II, and III, examine mechanisms of $K$-vacancy production in both partners in a heavy-ion collision, mainly for projectiles with $Z_1 \geq 35$ at selected energies between 10 and 500 MeV. We found it useful to describe the $K$-vacancy production mechanisms in terms of electron excitation from molecular orbitals (MO) by promotion[4] and by direct excitation.[5] As shown in I and II, the $K$-vacancy production cross sections for the higher (H)- and lower (L)-$Z$ collision partners can then be written as

$$\sigma_K(H) = \sigma(1s\sigma) + w\sigma(2p\sigma)\,, \tag{1}$$

$$\sigma_K(L) = (1-w)\sigma(2p\sigma) + \sigma_{K\text{-}L}\,, \tag{2}$$

where $\sigma(1s\sigma)$ and $\sigma(2p\sigma)$ are the cross sections for producing vacancies in the $1s\sigma$ and $2p\sigma$ MO, respectively, and $\sigma_{K\text{-}L}$ is the $K$-$L$ level matching contribution. In our model the $2p\sigma$ vacancies are shared on the outgoing part of the collision between the higher- and lower-$Z$ partners in the ratio[6]

$$w/(1-w) = e^{-2x}\,, \tag{3}$$

where

$$2x \equiv \pi(I_H^{1/2} - I_L^{1/2})/(\tfrac{1}{2}mv^2)^{1/2}\,. \tag{4}$$

Here $I_H$ and $I_L$ are the experimental $K$-shell binding energies of the higher- and lower-$Z$ partners, respectively, $v$ is the projectile velocity and $m$ the electronic mass. Close to symmetry $\sigma_K(H)$ and $\sigma_K(L)$ are dominated by $2p\sigma$-vacancy sharing (see II). Far from symmetry $\sigma_K(H)$ is dominated by direct $1s\sigma$ excitation (see III) and $\sigma_K(L)$ is dominated by the $K$-$L$ level matching cross section $\sigma_{K\text{-}L}$, as already noted in II and discussed in the

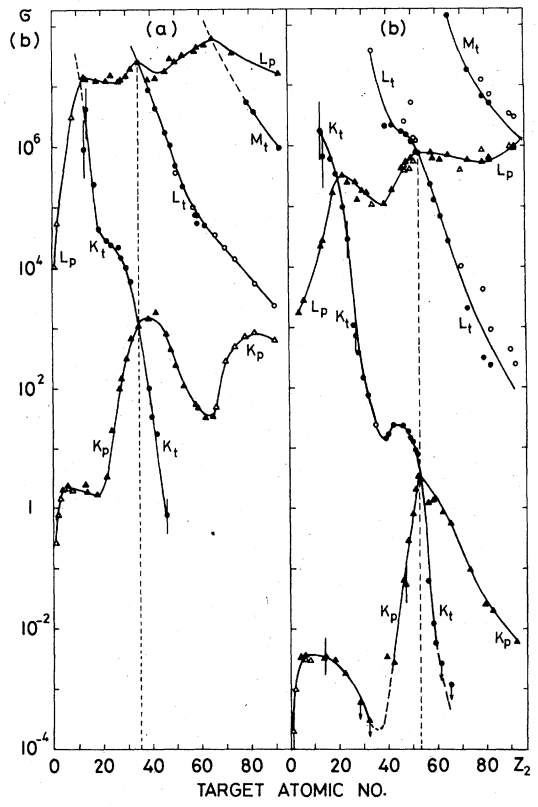


FIG. 1. Projectile ($p$) and target ($t$) vacancy-production cross sections for $K$, $L$, and $M$ shells: (a) 43-MeV $_{35}$Br projectiles, (b) 47-MeV $_{53}$I projectiles. Closed symbols from our work; in (a) open symbols from Refs. 7–9, 12; in (b) open symbols from Refs. 10–12. Typical errors are shown. Because single-vacancy fluorescence yields were used to obtain the cross sections, the $L$ and $M$ cross sections could be affected by large systematic errors. Curves are drawn to guide the eye. Dashed vertical lines indicate symmetric collisions.

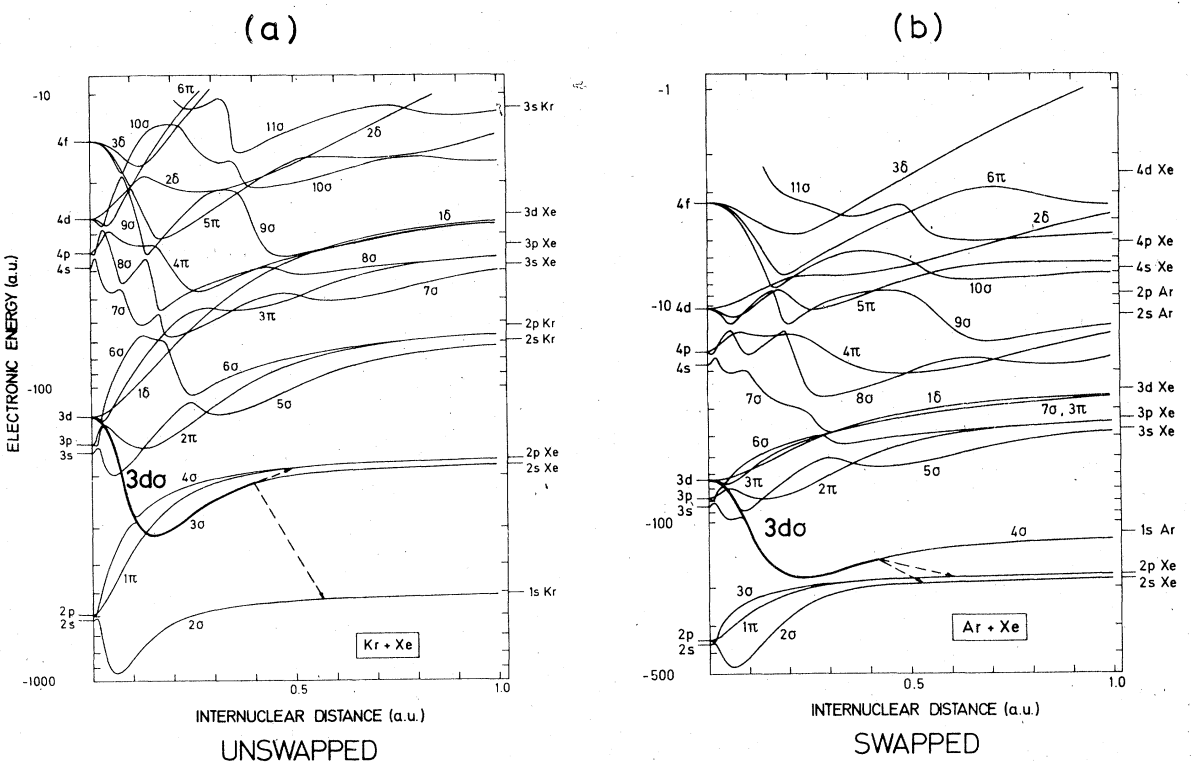


FIG. 2. Correlation diagrams for $_{36}Kr + _{54}Xe$ and $_{18}Ar + _{54}Xe$ collisions (Ref. 14): (a) unswapped case, (b) swapped case. The $3d\sigma$ MO is shown as a heavy curve. The dashed lines indicate the proposed vacancy-sharing transitions on the outgoing part of the collision.

present paper.

To avoid constant reference to I and II, we show in Figs. 1(a) and 1(b) typical projectile ($p$) and target ($t$) $K$, $L$, and $M$ cross sections for 43-MeV Br and 47-MeV I beams, plotted as a function of the target atomic number $Z_2$. The data is from our and other work.[7-12] In all cases, x-ray cross sections from solid targets were converted to vacancy cross sections using fluorescence yields from Ref. 13. Hence, much of the data shown in Fig. 1 cannot be interpreted simply in terms of single-collision cross sections.[2,3] We return to this point below. Here we draw attention only to the rapid fall of the target $K$ cross section for $Z_2 \lesssim 20$ for 43-MeV Br [Fig. 1(a)] and for $Z_2 \lesssim 35$ for 47-MeV I [Fig. 1(b)] and to the rise of the projectile $K$ cross section for $Z_2 \gtrsim 65$ for 43-MeV Br. We ascribe these cross section trends to $K$-$L$ level matching effects and attempt to explain them quantitatively.

In Sec. II a schematic vacancy-sharing model for $K$-$L$ level matching is introduced, which is compared with the data in Sec. III. Some remarks about the role of vacancy sharing in inner-shell vacancy production are made in Sec. IV. The data reduction is discussed in Appendix A. The potential role of electron capture in the data analysis is examined in Appendix B.

## II. VACANCY-SHARING MODEL

It is convenient to discuss our model for $K$-$L$ level matching with the aid of Fig. 2, taken from Ref. 14. Barat and Lichten[4] note that in an asymmetric collision, such as illustrated in Fig. 2(a), $L$ electrons from the higher-$Z$ partner (Xe) would be promoted along the $3d\sigma$ MO. [Their exact correlation scheme is slightly different from the one shown in Fig. 2(a). For a detailed discussion see Ref. 14.] If $Z_L$ is decreased, the $K$ level of the lower-$Z$ partner passes through the $L$ levels of the higher-$Z$ partner and the correlation of the $3d\sigma$ MO is "swapped" to the $1s(L)$ level [Fig. 2(b)]. Consequently there should be a large rise in the $K$ x-ray production of the lower-$Z$ partner, and a marked decrease in the $L$ x-ray production of the higher-$Z$ partner, as the swapping point is passed. Barat and Lichten[4] show that these ideas are in qualitative agreement with experiment ($Z_1 = 6$–$13$ bombardment of $Z_2 = 18$; see Ref. 15 for new data and interpretation). Armbruster *et al.*[16] give further evidence on this point.

An *ab initio* treatment of this problem is very complicated, since it involves the four MO's correlating to the $1s(L)$, $2s(H)$, $2p_{1/2}(H)$ and $2p_{3/2}(H)$ states. (From now on we omit the designations $H$

and $L$, since in this paper the $1s$ level always refers to the lower-$Z$ partner and the $2s,p$ levels always refer to the higher-$Z$ partner). To make the problem tractable we follow the suggestion of Foster *et al.*[17] that vacancy-sharing concepts[6] may be applicable here. We assume that on the outgoing part of the collision the $3d\sigma$ vacancies, however created, are shared between the above-mentioned four states and that direct excitation and ionization of the individual levels may be neglected:

$$\sigma(3d\sigma) = \sigma_K + \sigma_1 + \sigma_2 + \sigma_3 , \tag{5}$$

where $\sigma_K$ is the vacancy-production cross section in the $1s$ level and $\sigma_i$ $(i = 1, 2, 3)$ is the vacancy-production cross section in the $L_i$ subshell, as yet unaltered by Coster-Kronig transitions.[13] We write, for the $3d\sigma$-vacancy transfer probabilities,

$$P_0 + P_a + P_b + P_c = 1 , \tag{6}$$

where we set, in accordance with the correlations on Fig. 2, for the unswapped case:

$$P_0 = \sigma_1/\sigma(3d\sigma) , \tag{7a}$$

$$P_a = \sigma_K/\sigma(3d\sigma) , \tag{7b}$$

$$P_b = \sigma_2/\sigma(3d\sigma) , \tag{7c}$$

$$P_c = \sigma_3/\sigma(3d\sigma) ; \tag{7d}$$

for the swapped case:

$$P_0 = \sigma_K/\sigma(3d\sigma) , \tag{8a}$$

$$P_a = \sigma_1/\sigma(3d\sigma) , \tag{8b}$$

$$P_b = \sigma_2/\sigma(3d\sigma) , \tag{8c}$$

$$P_c = \sigma_3/\sigma(3d\sigma) . \tag{8d}$$

Unfortunately, vacancy-sharing models have been worked out only for the two-state problem. Therefore, we break down the four-state problem into a set of two-state problems. We attempt to use a two-level model to compute the individual ratios $P_a/P_0, P_b/P_0, P_c/P_0$. If there is relatively weak coupling between the MO's represented by $a$, $b$, and $c$, such a procedure may be justifiable. To calculate each ratio we use the exponential coupling model of Nikitin,[18] which has sufficient flexibility to accomodate a variety of functional forms for the dependence of level separation on internuclear distance.[19] (The Demkov model[6,20] for constant level separation is a special case of the Nikitin model.)

Following our procedure, we set

$$P_k/P_0 = P_{0k}/(1 - P_{0k}) , \quad k = a, b, c , \tag{9}$$

where $P_{0k}$ is the vacancy-transfer fraction from the $3d\sigma$ MO to level $k$, as given by the two-state model of Nikitin[18]:

$$P_{0k} = \frac{\exp[2\lambda_k(1 + \cos\theta_k)] - 1}{\exp(4\lambda_k) - 1} . \tag{10}$$

The parameter $2\lambda_k$ is identical to the parameter $2x$ of Eq. (4), so that we set[6]

$$2\lambda_k = \pi \left| I_0^{1/2} - I_k^{1/2} \right| / (\tfrac{1}{2} m v^2)^{1/2} \tag{11}$$

and use $\theta_k$ as a free parameter. For $\theta_k = 90°$, Eq. (9) reduces to the vacancy-sharing ratio $w/(1-w)$, Eq. (3), based on the Demkov model. In principle, a less ambiguous approach would be to adjust the parameters available in the Nikitin model[18] to the actual MO energy-separation dependence on internuclear distance.[19] This would require extensive many-electron MO energy computations. To obtain the individual vacancy-sharing probabilities, we combine Eqs. (6) and (9),

$$P_k = \frac{P_{0k}}{(1 - P_{0k})\left[1 + \sum_{n=a,b,c} P_{0n}/(1 - P_{0n})\right]} , \quad k = a, b, c , \tag{12}$$

$$P_0 = \left(1 + \sum_{n=a,b,c} \frac{P_{0n}}{(1 - P_{0n})}\right)^{-1} , \tag{13}$$

and substitute Eq. (10).

## III. COMPARISON WITH EXPERIMENT

### A. Vacancy fractions

As discussed in Appendix A, one can experimentally determine the cross section $\sigma_K$ for $K$-vacancy production in the lower-$Z$ partner [Eq. (A12)] and the total $L$-vacancy production cross section $\sigma_L (= \sigma_1 + \sigma_2 + \sigma_3)$ in the higher-$Z$ partner [Eq. (A13)]. In the spirit of our model we then set

$$\sigma(3d\sigma) = \sigma_K + \sigma_L . \tag{14}$$

From most of the data available to us, it was not possible to extract the individual primary vacancy cross sections $\sigma_1$, $\sigma_2$, and $\sigma_3$, but only certain combinations [Eqs. (A8), (A10)]:

$$\sigma_2'' = \sigma_2 + (f_{12} + r)\sigma_1 , \tag{15}$$

$$\sigma_3' = \sigma_3 + f_{23}\sigma_2 + (f_{12}f_{23} + f_{13})\sigma_1 . \tag{16}$$

Here $f_{ij}$ is the Coster-Kronig transition probability from subshell $L_i$ to subshell $L_j$ and $r$ is a complicated ratio [Eq. (A11)] which, fortunately, has a nearly constant value of 0.45 (Appendix A 2) in the region where it is of importance (i.e., if $\sigma_1 \simeq \sigma_2$). Therefore, from experiment one can obtain the vacancy ratios [Eqs. (A15)–(A17)]

$$v_K = \sigma_K/(\sigma_K + \sigma_L) , \tag{17}$$

$$v_3' = \sigma_3'/(\sigma_K + \sigma_L) , \tag{18}$$

$$v_2'' = \sigma_2''/(\sigma_K + \sigma_L) . \tag{19}$$

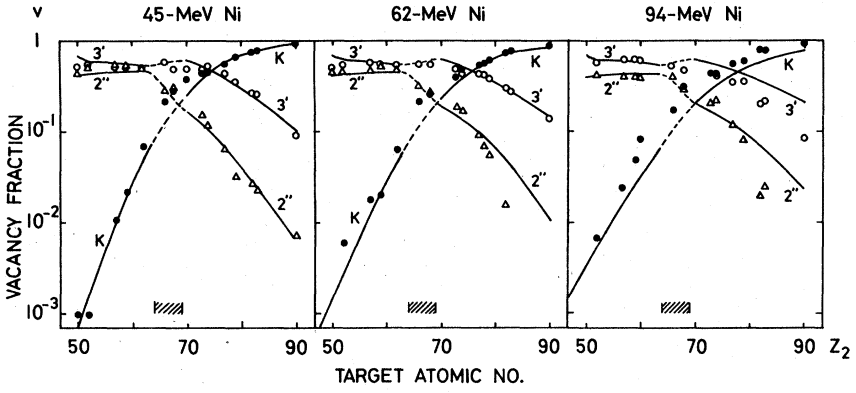


FIG. 3. Comparison of experimental and computed vacancy fractions for collisions of $_{28}$Ni projectiles with various targets. The vacancy fractions are defined in Eqs. (17)–(19). The $K$-vacancy fraction $v_K$ refers to the lower-$Z$ partner (Ni), the $L$-vacancy fractions $v_2''$ and $v_3'$ refer to the higher-$Z$ partner. Data from Refs. 7–9. A few points have been interpolated. Systematic errors up to 50% may be expected (Appendix A). Curves are computed vacancy fractions [Eqs. (20)–(25)]. The $K$-$L$ swapping region is indicated on the $Z_2$ axis by the hashing. The computed curves are connected by dashed lines across the swapping region. The unswapped region is on the left of each figure, the swapped region on the right.

The model predictions (Sec. II) for the same ratios are, in the unswapped case,

$$v_K = P_a , \tag{20}$$

$$v_3' = P_c + f_{23}P_b + (f_{12}f_{23} + f_{13})P_0 , \tag{21}$$

$$v_2'' = P_b + (f_{12} + r)P_0 , \tag{22}$$

and, for the swapped case,

$$v_K = P_0 , \tag{23}$$

$$v_3' = P_c + f_{23}P_b + (f_{12}f_{23} + f_{13})P_a , \tag{24}$$

$$v_2'' = P_b + (f_{12} + r)P_a . \tag{25}$$

Following the discussion in Appendix A 2 we use single-vacancy values for the Coster-Kronig transition probabilities,[13] fluorescence yields,[13] and radiative widths,[21] even though systematic errors as large as 50% may then be expected in the vacancy fractions. The actual errors are probably smaller, because we form cross section ratios, so that there is some error cancellation. In the swapped case one finds $P_a \ll P_b$; hence the exact value of $r$ plays no role in that case [Eq. (25)].

Figures 3–5 give a comparison of the experimental vacancy fractions, Eqs. (17)–(19), with the vacancy fractions of Eqs. (20)–(25) computed by our model, based on Eqs. (10)–(13). For the Ni and Br beams, we made use of unpublished data from Refs. 7–9; for the I beam we used our own data. In the spirit of the simple model we are using, we assumed that for a given projectile the parameters $\theta_a$, $\theta_b$, and $\theta_c$ in Eq. (10) are indepen-

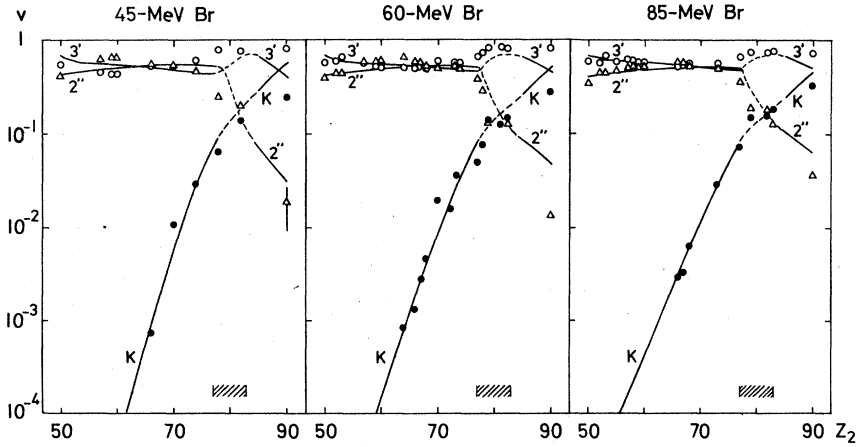


FIG. 4. Same as Fig. 3, for $_{35}$Br projectiles.

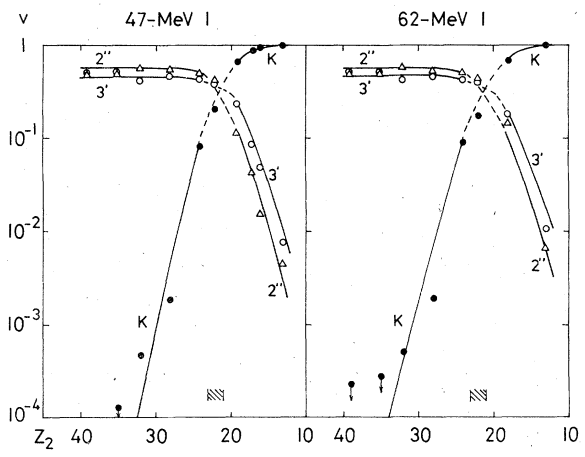


FIG. 5. Same as Fig. 3, for $_{53}$I projectiles. Here the target atom is the lower-$Z$ partner; to keep the unswapped case on the left side of each figure, $Z_2$ is plotted increasing to the left. Data from our work.

dent of projectile energy or target $Z$, except that in the swapped and unswapped cases different values of $\theta$ were permitted, because of the different level correlations (Fig. 2). By trial and error a set of $\theta$ values was found which produced a good overall fit of the model to the data. These $\theta$ values are listed in Table I.[22] The value of $\theta_a$ in the swapped case cannot be determined, since $P_a \ll P_b$. Hence, we set $\theta_a = 90°$ in that case. We have refrained from using our model in the target-$Z$ region where the lower-$Z$ 1$s$ level lies *between* the higher-$Z$ 2$s$ and $2p_{3/2}$ levels. In Figs. 3–5, the curves calculated for the swapped and unswapped regions are simply connected by dashed lines.

The work of Tanis[23] on Br collisions with rare-earth targets allows the extraction of the $L$-subshell cross sections $\sigma_1$ and $\sigma_2'$ [Eq. (A7)], as well as $\sigma_3'$ [Eq. (16)], where

$$\sigma_2' = \sigma_2 + f_{12}\sigma_1 . \tag{26}$$

Therefore, in addition to the vacancy fraction $v_3'$ given by Eq. (18), one can obtain, experimentally, the fractions

$$v_1 = \sigma_1/(\sigma_K + \sigma_L) , \tag{27}$$

TABLE I. Overall best fit values of $\theta$ parameters.

| Projectile[a] | Unswapped case $\theta_a$ | $\theta_b$ | $\theta_c$ | Swapped case $\theta_a$ | $\theta_b$ | $\theta_c$ |
|---|---|---|---|---|---|---|
| Ni | 119° | 72° | 54° | 90° | 72° | 54° |
| Br | 119° | 72° | 54° | 90° | 72° | 54° |
| I | 94° | 85° | 76° | 90° | 85° | 76° |

[a]The $\theta$ parameters are assumed to be independent of bombarding energy or target-$Z$.

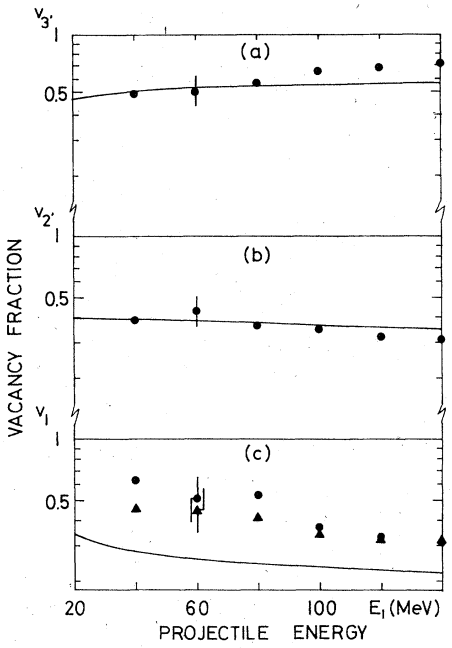


FIG. 6. Comparison of experimental and computed vacancy fractions for 40–140-MeV $_{35}$Br + $_{62}$Sm collisions. Data from Ref. 23. The $L$-vacancy ratios $v_1$, $v_2'$ and $v_3'$ for Sm are defined in Eqs. (27), (28), and (18), respectively. In the case of $v_1$, figure (c), the cross section $\sigma_1$ has been obtained in two different ways: from $\sigma_{\beta 3} + \sigma_{\beta 4}$ (circles), using Eq. (A3), and from $\sigma_{\gamma 2} + \sigma_{\gamma 3}$ (triangles), using Eq. (A6).

$$v_2' = \sigma_2'/(\sigma_K + \sigma_L) . \tag{28}$$

These fractions can be compared with our model through the relations, for the unswapped case,

$$v_1 = P_0 , \tag{29}$$

$$v_2' = P_b + f_{12}P_0 , \tag{30}$$

as well as Eq. (21). The results of this more stringent, independent test of our model are shown in Fig. 6 for 40–140-MeV Br + Sm collisions, using the $\theta$ values from Table I. The overall agreement between experiment and our model is satisfactory, although some finer variations found by Tanis in certain cross section ratios,[23] such as $\sigma_{\beta(1)}/\sigma_\alpha$, cannot be reproduced by the model.

### B. Discussion

It is remarkable that with so few bombarding-energy- and $Z_2$-independent values of the $\theta$ parameters (Table I) the trends of the vacancy fractions with target $Z$ and bombarding energy are quantitatively reproduced (Figs. 3–6). This is reminiscent of the fact that the Demkov formula is so successful for $2p\sigma$-vacancy sharing between the 1$s$ levels of the collision partners.[2,6] (Also the good

quantitative agreement may be an *a posteriori* justification for representing a four-level problem by a series of two-level problems.)

The angles $\theta$ in the Nikitin model[18] are associated with the expansion coefficients of an MO wave function into atomic wave functions of the two partners. In the Demkov formulation, $\theta = 90°$. This corresponds to a representation of the $(2p\sigma)$ MO as an antisymmetric linear combination of two identical atomic states. In the present case, the vacancy sharing takes place between levels of dissimilar configurations, namely $1s$ and $2s$, $2p$. If we try again to associate the angles $\theta$ with expansion coefficients of the feeding $3d\sigma$ MO into atomic orbitals we will, in general, expect $\theta \neq 90°$. Hence, $\theta$ appears as an additional parameter. We have attempted to cast the MO wave function (using the formulation of Helfrich and Hartmann[24] for the two-center Coulomb problem) into an atomic orbital form appropriate to the Nikitin model,[18] but we were unable to reproduce the empirical values of the $\theta$ parameters. However, we believe that the empirical constancy of the $\theta$ parameter across the entire level matching region (similarly as in the Demkov case) is connected with a remarkable constancy of the inner part of the MO wave function as the ratio $Z_H/Z_L$ is varied.

For the theoretical determination of the $\theta_k$ an approach similar to that of Bőving[19] may be more successful, although at the expense of giving up a simple interpretation of the $\theta_k$.

We close this section by commenting on the correlation schemes of Refs. 4 and 14. In the swapped case, the schemes are identical, but in the unswapped case the Barat-Lichten[4] scheme correlates the $3d\sigma$ MO to the $2p_{3/2}$ level, whereas the scheme of Eichler *et al.*,[14] shown in Fig. 2a, correlates the $3d\sigma$ MO to the $2s_{1/2}$ level of the higher-$Z$ partner. Originally we had hoped that the experimental vacancy fractions would distinguish between the two schemes.[25] Unfortunately, it turns out that after suitable redefinition of the probabilities in Eq. (7) (i.e., interchanging $P_0$ and $P_c$), the $\theta$ parameters can be adjusted to make the Barat-Lichten scheme[4] fit equally well to the data shown in Figs. 3–6, as the scheme of Ref. 14 used in the present paper. Therefore, other means will have to be employed to distinguish between the two correlation schemes.

### C. $3d\sigma$-vacancy cross section

In our model the $3d\sigma$-vacancy cross section can be obtained from experiment by simply adding the $K$- and $L$-vacancy production cross sections [Eq. (14)]. Figures 7–9 show these cross sections for Ni, Br, and I projectiles of selected energies. The Ni and Br data are from Refs. 7–9; the I data

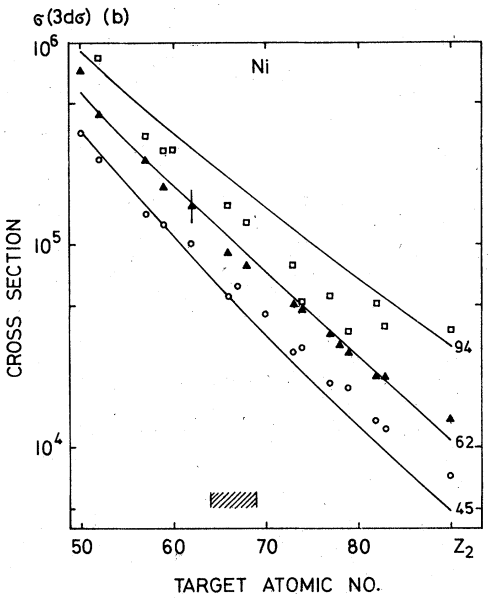


FIG. 7. Summed lower-$Z$, $K$-, and higher-$Z$, $L$-vacancy production cross sections for $_{28}$Ni beam as a function of target $Z$. Data from Refs. 7–9. According to the present model, the sum cross section represents the $3d\sigma$-vacancy production cross section. Swapping region is indicated by hashing. Curves, modified BEA proposal of Ref. 17, normalized as discussed in text. Bombarding energy in MeV is indicated next to each curve. Minimum (statistical) error is shown.

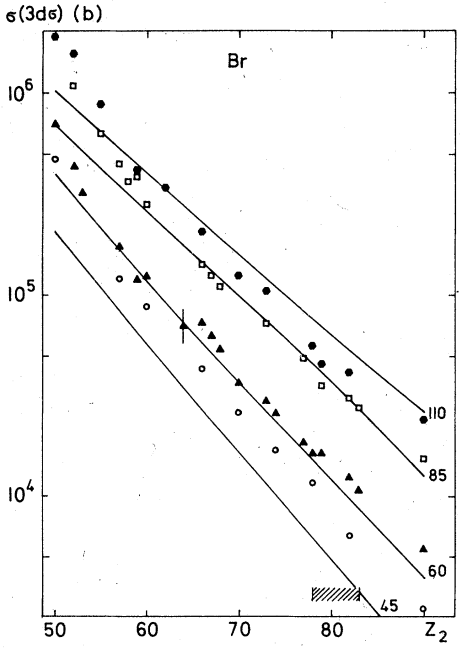


FIG. 8. Same as Fig. 7, for $_{35}$Br beam.

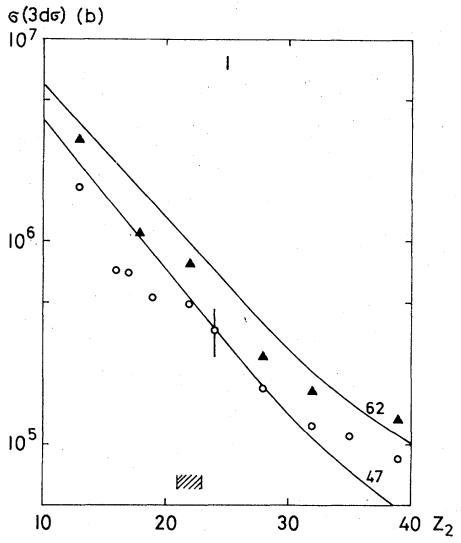


FIG. 9. Same as Fig. 7, for $_{53}$I beam. Data from our work.

are from our work. The most noteworthy feature of these data is their smooth behavior across the $K$-$L$ swapping region (hashed lines along $Z_2$ axis). This is characteristic of vacancy sharing, since in the generation of the primary ($3d\sigma$) vacancies resonance effects due to level matching between outgoing collision partners play no role.

Looking at Fig. 2 and recalling the discussion in II,[2] there are at least[11] three different ways of producing $3d\sigma$ vacancies: (1) by direct (Coulomb) excitation from the $3d\sigma$ MO,[17] (2) by multistep processes such as $3d\sigma$-$3d\pi$ electron promotion[4] followed by $3d\pi$ coupling to vacant states in a single collision, analogous to the $2p\sigma$-$2p\pi$-$3p\pi$ coupling discussed by Fastrup,[26] and (3) by coupling projectile $L$ or $M$ vacancies produced in prior collisions to the $3d\pi$ MO, followed by $3d\sigma$-$3d\pi$ electron promotion. Hagmann has drawn attention also to possible radial-coupling processes between the $3d\sigma$ MO and other $\sigma$ orbitals which it crosses at small internuclear distances.[11]

Process (3) is quite similar to the multiple-collision process examined in II.[2] In the present case, though, one must carefully distinguish whether the projectile is the lower-$Z$ or the higher-$Z$ collision partner. If the projectile is the lower-$Z$ partner, projectile $2p$ vacancies correlate to the $3d\pi$ MO only if the projectile $2p$ levels lie below the target $M$ levels [Fig. 2(a)], but not if they lie above the target $M$ levels [Fig. 2(b)]. Hence, as the $L$-$M$ swapping region is crossed, a sharp drop in the $3d\sigma$ vacancy production cross section is expected. For Ni and Br, the $L$-$M$ swapping regions correspond to $Z_2 \simeq 52$–$58$ and $Z_2 \simeq 62$–$71$, respectively. In Figs. 7 and 8 no marked decrease in $3d\sigma$-vacancy production above these $Z_2$ ranges is apparent, suggesting that multiple-collision effects are not important here.

If the projectile is the higher-$Z$ partner, as for the I projectile data shown in Fig. 9, projectile $M$ vacancies have many possibilities to couple into the $3d\sigma$ MO at small internuclear distances[11] [Figs. 2(a) and (b)]. Therefore, a smooth $Z_2$ dependence is expected for $3d\sigma$-vacancy production across the $L$-$M$ swapping region ($Z_2 \simeq 25$–$29$). This is found (Fig. 9), but leads to no special conclusion.

To distinguish between the single-collision processes (1) and (2) mentioned above, i.e., direct excitation or multiple-step promotion, one would need to perform experiments with gas targets, using projectiles with different charge states. In the absence of such work and for general orientation we show in Figs. 7–9 curves obtained from the proposals of Hansen[27] and of Foster *et al.*,[17] that one should substitute the united-atom (UA) binding energy into the binary-encounter approximation (BEA) formula in order to simulate the binding-energy effect in inner-shell ionization. Since we have no evidence for important multiple-collision effects, the application of these "theoretical" single-collision cross section estimates to $3d\sigma$-vacancy production should be justified. Therefore we substituted the UA $3d$ binding energy in the equation on page 1947 of Ref. 17, using the BEA $2p$ function from Hansen.[27] But we had to divide the resulting cross sections by 20, 7, and 5 in order to obtain the curves in Figs. 7, 8, and 9, respectively. One sees that the $Z_2$ and bombarding-energy dependence of the $3d\sigma$ cross section is qualitatively reproduced by this prescription. Clearly, no meaningful conclusion about the importance of direct ionization in $3d\sigma$-vacancy production can be drawn, in view of the arbitrary scaling which had to be applied to computed cross sections.

## IV. SUMMARY

### A. $K$-$L$ level matching

The model we have used to describe the $K$ cross section of the lower-$Z$ partner and the $L$ cross sections of the higher-$Z$ partner in the $K$-$L$ level matching region assumes that vacancies are initially formed in the $3d\sigma$ MO and then shared between the collision partners on the outgoing part of the collision. A breakdown of the four-state problem into two-state problems using the model of Nikitin[18] appears to give a good representation of the target-$Z$ and bombarding-energy dependence of the various sharing ratios (Figs. 3–6). It would be desirable to make an *ab initio* four-state calculation of the sharing ratios along the lines of the

calculations by Taulbjerg and Briggs for $2p\sigma$-vacancy sharing.[28]

In our model the steep target-$Z$ dependence of the $K$-vacancy cross section for the lower-$Z$ partner far from symmetry, illustrated in Fig. 1, can be understood in terms of the exponential dependence of the $3d\sigma$-vacancy transfer probability on the energy separation between the $1s(L)$ and $2s,p(H)$ levels [Eqs. (10) and (11)]. The $Z_2$-dependence of the $3d\sigma$ cross section (Figs. 7–9) plays only a minor role.

We have not been able to pinpoint the dominant process of $3d\sigma$-vacancy formation, although we present evidence which appears to indicate that multiple-collision effects do not play a dominant role.

### B. Role of vacancy sharing in inner-shell vacancy formation

The general trends of $K$, $L$, and $M$ cross sections shown in Fig. 1 are discussed by Armbruster *et al.*[16] on the basis of the promotion model of Barat and Lichten.[4] If one supplements their ideas with the concept of vacancy sharing, one can obtain a more quantitative explanation of the cross section trends for inner-shell vacancy formation.[11] It appears that near each level matching region the dominant process consists of the (primary) vacancy formation in a highly promoted MO, followed by the (secondary) sharing of these vacancies between the levels of the two collision partners. The primary MO's are[4,14] $2p\sigma$, $4f\sigma$, and $6h\sigma$, for $K$-$K$, $L$-$L$, and $M$-$M$ level matching, respectively, $3d\sigma$ and $5g\sigma$ for $K$-$L$ and $L$-$M$ level matching, respectively, and $4f\sigma$ for $K$-$M$ level matching. By summing the vacancy cross sections for both collision partners near each level matching region one can obtain the primary vacancy cross sections. This has been done in Figs. 10(a) and 10(b) for the data shown in Figs. 1(a) and 1(b). The heavy lines give the primary cross sections. The thin lines give the vacancy-shared cross sections of the two collision partners, without taking into account subshell branching. Since only single-vacancy values of the fluorescence yields have been used,[13] the $L$ and $M$ cross section trends must be taken as qualitative, rather than quantitative. (There is also considerable scatter in some of the higher-shell x-ray data.) Nevertheless, it is pleasing that the cross sections for primary $3d\sigma$ formation, obtained from the target-$K$-projectile-$L$ and target-$L$-projectile-$K$ level matching regions, appear to lie on a coherent curve, shown by the heavy dashed line in Fig. 10.

From Fig. 10 it is apparent that in between the various level matching regions each collision partner can obtain vacancies from more than one primary process. [This feature is incorporated in Eqs. (1) and (2).] Other coupling processes may then also become important.

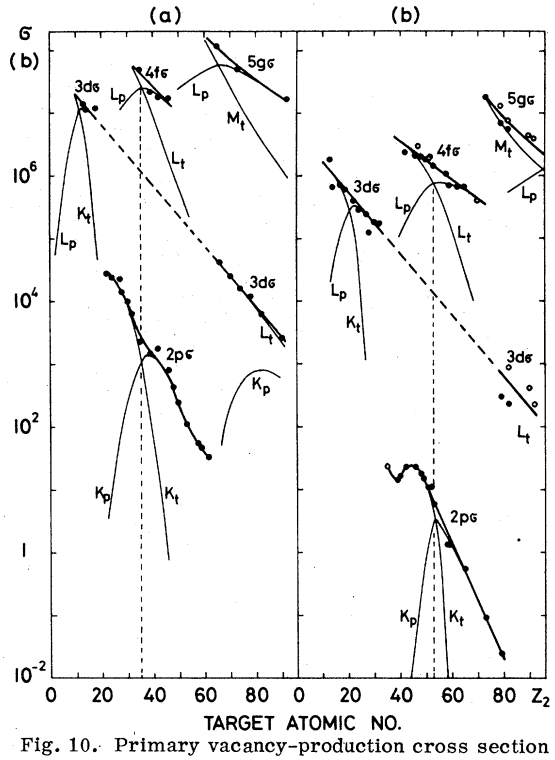


Fig. 10. Primary vacancy-production cross section for (a) 43-MeV $_{35}$Br and (b) 47-MeV $_{53}$I projectiles. Near each level-matching region the summed projectile ($p$) and target ($t$) vacancy cross section is given in heavy lines. The two regions of $3d\sigma$ excitation have been arbitrarily connected. The thin lines give the individual cross sections. See Fig. 1 for data points. Vertical dashed lines indicate symmetric collisions. Curves are drawn to guide the eye.

In very asymmetric collisions, i.e., $Z_1 \lesssim 7$, $Z_2 \gtrsim 30$, the vacancy-sharing model may break down for the higher-$Z$ collision partner. It seems then more appropriate to use Coulomb excitation from atomic orbitals, with appropriate corrections for molecular influences.[29,30] No doubt it will be possible eventually to incorporate into the theory a smooth transition from the atomic-orbital to the molecular-orbital model.[3]

### ACKNOWLEDGMENTS

One of us (W. E. Meyerhof) is very grateful to B. Crasemann for clarifying the formulation of $L$-shell vacancy cross sections. This work was supported in part by the National Science Foundation, by the U. S. Energy Research and Development Administration [Contract No. AP(04-3)-115P/A84] and by SRI International Independent Research and Development Funds.

## APPENDIX A: DATA REDUCTION

### 1. Vacancy fractions

In order to interpret available $K$- and $L$-x-ray cross section data with our model (Sec. II), it is convenient to extract, as far as possible, information about the initial vacancy formation in the $L_1$, $L_2$ and $L_3$ subshells of the higher-$Z$ collision partner. Although for projectiles with $Z_1 \lesssim 3$ quite detailed $L$ spectra can be obtained and analyzed (see, e.g., Ref. 31), if higher-$Z$ projectiles are used, the spectral lines are broadened by multiple-ionization effects.[32,33] For Ni, Br, and I projectiles, one finds partially resolved groups of lines,[7-11] called here $Ll, L\alpha, L\beta(1), L\beta(2), L\gamma 1$, $L\gamma(2)$. It is not difficult to express the x-ray cross sections for the major components of each group in terms of the primary $L$-subshell vacancy-production cross sections $\sigma_1, \sigma_2, \sigma_3$ or the Coster-Kronig altered cross sections $\sigma_2'$ and $\sigma_3'$, defined below[11,13,32]:

$$\sigma_l = \sigma_3' \omega_3 \Gamma_{3,M1}/\Gamma_3 , \tag{A1}$$

$$\sigma_\alpha = \sigma_3' \omega_3 (\Gamma_{3,M4} + \Gamma_{3,M5})/\Gamma_3 , \tag{A2}$$

$$\sigma_{\beta(1)} \equiv \sigma_{\beta 1} + \sigma_{\beta 3} + \sigma_{\beta 4} = \sigma_2' \omega_2 \Gamma_{2,M4}/\Gamma_2 + \sigma_1 \omega_1 (\Gamma_{1,M2} + \Gamma_{1,M3})/\Gamma_1 , \tag{A3}$$

$$\sigma_{\beta(2)} \equiv \sigma_{\beta 2} + \sigma_{\beta 15} = \sigma_3' \omega_3 (\Gamma_{3,N4} + \Gamma_{3,N5})/\Gamma_3 , \tag{A4}$$

$$\sigma_{\gamma 1} = \sigma_2' \omega_2 \Gamma_{2,N4}/\Gamma_2 , \tag{A5}$$

$$\sigma_{\gamma(2)} \equiv \sigma_{\gamma 2} + \sigma_{\gamma 3} = \sigma_1 \omega_1 (\Gamma_{1,N2} + \Gamma_{1,N3})/\Gamma_1 . \tag{A6}$$

Here $\omega_i$ and $\Gamma_i$ are the fluorescence yield and total radiative width of the subshell $L_i$ and $\Gamma_{i,k}$ is the partial radiative width for the transition from a higher subshell $k$ to the subshell $L_i$. The Coster-Kronig altered cross sections are defined by

$$\sigma_2' = \sigma_2 + f_{12}\sigma_1 , \tag{A7}$$

$$\sigma_3' = \sigma_3 + f_{23}\sigma_2 + (f_{12}f_{23} + f_{13})\sigma_1 , \tag{A8}$$

where $f_{ij}$ is the Coster-Kronig transition probability from subshell $L_i$ to $L_j$. In Eq. (A3) the $L\beta 3, 4$ contribution is included in the group $L\beta(1)$ because it cannot be resolved from $L\beta 1$ for high-$Z$ projectiles,[10,11] except by a very careful analysis of line shapes.[23]

In principle, it should be possible to solve three equations, e.g. Eqs. (A2), (A3), and (A6), for $\sigma_1$, $\sigma_2'$, and $\sigma_3'$, if the fluorescence yields[13] and radiative widths[21] are known. In practice, in most of the data available to us,[9] the $L\gamma 2, 3$ lines are not resolved from $L\gamma 1$, so that it is not possible to make use of Eq. (A6). Hence, we introduce a mixed, altered subshell cross section $\sigma_2''$, defined by

$$\sigma_{\beta(1)} = \sigma_2'' \omega_2 \Gamma_{2,M4}/\Gamma_2 , \tag{A9}$$

where

$$\sigma_2'' = \sigma_2' + r\sigma_1 = \sigma_2 + (f_{12} + r)\sigma_1 \tag{A10}$$

$$r \equiv \frac{\omega_1(\Gamma_{1,M2} + \Gamma_{1,M3})/\Gamma_1}{\omega_2 \Gamma_{2,M4}/\Gamma_2} . \tag{A11}$$

For comparison with our model, for the higher-$Z$ partner the altered cross sections $\sigma_2''$ and $\sigma_3'$ can be extracted from the experimental x-ray cross sections $\sigma_{\beta(1)}$ and $\sigma_\alpha$, using Eqs. (A9) and (A2). For the lower-$Z$ partner we can obtain the $K$-vacancy cross section $\sigma_K$ from

$$\sigma_K = \sigma_{Kx}/\omega_K , \tag{A12}$$

where $\sigma_{Kx}$ is the experimental $K$ x-ray cross section and $\omega_K$ the $K$ fluorescence yield.[13]

The model of Sec. II provides only the cross section ratios, Eqs. (7) and (8), of the subshell cross sections to the total $3d\sigma$ cross section. Therefore, we need to extract also a total $L$-vacancy cross section $\sigma_L$ from the total experimental $L$ x-ray cross section $\sigma_{Lx}$:

$$\sigma_L \equiv \sigma_1 + \sigma_2 + \sigma_3 = \sigma_{Lx}/\tilde{\omega}_L , \tag{A13}$$

where

$$\sigma_{Lx} = \sigma_l + \sigma_\alpha + \sigma_{\beta(1)} + \sigma_{\beta(2)} + \sigma_{\gamma 1} + \sigma_{\gamma(2)} , \tag{A14}$$

and $\tilde{\omega}_L$ is a suitably defined average fluorescence yield.[13] We have been able to show that for the collision systems of interest here $\tilde{\omega}_L$ can be set equal to the $L_3$-subshell fluorescence yield $\omega_3$ with less than 10% error.

Finally, for comparison with the model we define the experimentally extracted vacancy fractions

$$v_K = \sigma_K/(\sigma_K + \sigma_L) , \tag{A15}$$

$$v_3' = \sigma_3'/(\sigma_K + \sigma_L) , \tag{A16}$$

$$v_2'' = \sigma_2''/(\sigma_K + \sigma_L) , \tag{A17}$$

where $\sigma_3'$, $\sigma_2''$, and $\sigma_L$ refer to the higher-$Z$ collision partner and $\sigma_K$ refers to the lower-$Z$ partner. Due to the particular definitions of $\sigma_3'$ and $\sigma_2''$ [Eqs. (A8) and (A10)], the sum $v_K + v_3' + v_2''$ does not add to unity.

### 2. Cross section ratios

Because of the difficulty of estimating fluorescence yields, Coster-Kronig transition probabilities and radiative widths for projectile and target atoms in solid targets,[34] for sake of definitiveness we prefer to use tabulated single-vacancy values[13,21] for these quantities, rather than to make estimates of the true values.[11] A partial check on the accuracy of this procedure can be obtained by comparing x-ray cross section ratios[10,23,32]

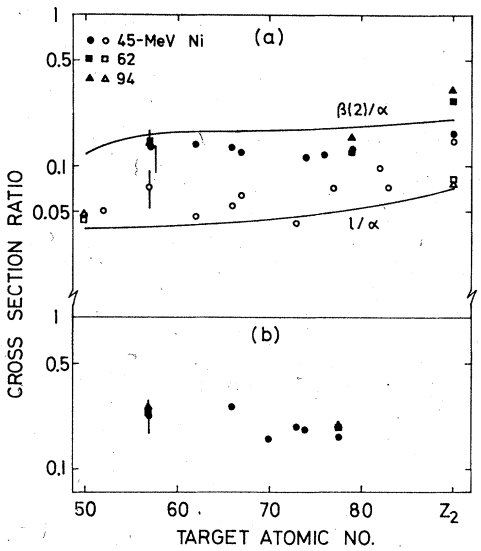


FIG. 11. $L$ cross section ratios for $_{28}$Ni projectiles. Data from Ref. 9. (a) $\sigma_{\beta(2)}/\sigma_{\alpha'}$ and $\sigma_1/\sigma_\alpha$. (b) $[\sigma_{\gamma 1}+\sigma_{\gamma(2)}]/\sigma_{\beta(1)}$. For definition of cross sections see Eqs. (A1)–(A6). Typical errors are shown. Curves in (a) use single-vacancy branching ratios of Scofield (Ref. 21).

with the tabulations. For example, from Eqs. (A1), (A2), and (A4) one obtains

$$\sigma_1/\sigma_\alpha = \Gamma_{3,M1}/(\Gamma_{3,M4}+\Gamma_{3,M5})\,, \tag{A18}$$

$$\sigma_{\beta(2)}/\sigma_\alpha = (\Gamma_{3,N4}+\Gamma_{3,N5})/(\Gamma_{3,M4}+\Gamma_{3,M5})\,. \tag{A19}$$

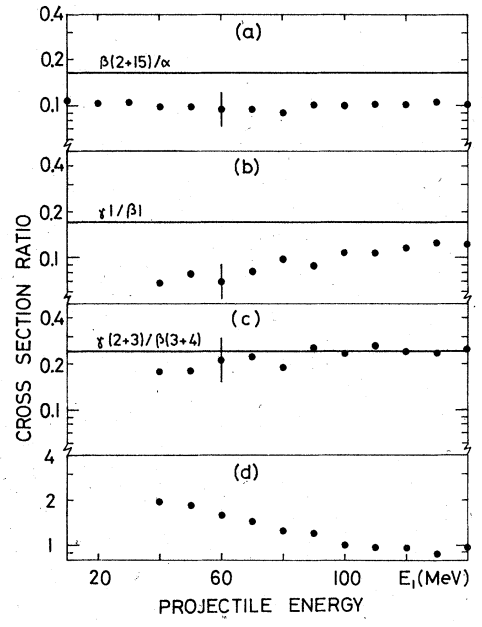


FIG. 12. $L$ cross section ratios for $_{35}$Br + $_{62}$Sm collisions as a function of Br projectile energy. Data from Ref. 23. (a) $\sigma_{\beta(2)}/\sigma_{\alpha'}$. (b) $\sigma_{\gamma 1}/\sigma_{\beta 1}$. (c) $\sigma_{\gamma(2)}/(\sigma_{\beta 3}+\sigma_{\beta 4})$. (d) $\sigma_{\gamma(2)}/\sigma_{\gamma 1}$. In (a), (b), and (c) single-vacancy branching ratios of Scofield (Ref. 21) are given.

Figure 11(a) compares experimental and single-vacancy[21] values of various *target* ratios (A18) and (A19) produced in collisions with 45–94-MeV Ni beams.[9] For a given target, there is relatively little bombarding-energy dependence of the branching ratios to a given $L$ subshell. This agrees with careful measurements by Tanis,[23] samples of which are shown in Fig. 12(a)–(c). Datz *et al.*[10] find for the 15–60-MeV I *projectile* ratios (A18) and (A19) the values $0.07 \pm 0.01$ and $0.165 \pm 0.02$, respectively, independent of $Z_2$, compared to the single-vacancy values[21] 0.038 and 0.14. Therefore, it appears that experimental branching ratios to a given $L$ subshell lie within 50% of the single-vacancy values, despite definite systematic deviations. Using single-vacancy values for the radiative widths, one must then count on possible systematic errors up to 50% for the experimental vacancy fractions. Considering though, that we wish to explain trends of vacancy fractions extending over factors $10^2$ to $10^3$ (Sec. III), such an accuracy should be acceptable.

One can also examine cross section ratios to different $L$ subshells. Datz *et al.*[10] find for the 15–60-MeV I *projectile* ratio $\sigma_{\gamma(2)}/\sigma_{\gamma 1}$ the value $1.1 \pm 0.4$, independent of $Z_2$. Tanis[23] finds for the same *target* ratio in 40–140-MeV Br + Sm collisions a similar magnitude, but some variation with bombarding energy [Fig. 12(d)]. Therefore, from Eqs. (A5) and (A6) we conclude that the ratio $\sigma_1\omega_1/(\sigma_2'\omega_2)$ is only slightly dependent on $Z_H$ and bombarding energy. The same conclusion can be drawn from the $Z_2$ independence of the *target* ratio $[\sigma_{\gamma 1}+\sigma_{\gamma(2)}]/\sigma_{\beta(1)}$ for 45–94-MeV Ni beams,[9] shown in Fig. 11(b).

The approximate constancy of the ratios (A18) and (A19) and the preceding conclusions lead us also to use single-vacancy values for the fluorescence yields[13] and widths[21] in Eq. (A11). This results in an approximately constant value $r \simeq 0.45$ in Eq. (A10) over most of the region of interest in our work.

## APPENDIX B: ELECTRON CAPTURE

Betz[35] and Bell[36] have drawn attention to the fact that capture of target electrons into projectile vacancies may affect projectile and target x-ray yields. In the present context, electron capture can make itself felt in two different ways. First, it can influence the production of $3d\sigma$ vacancies, if these vacancies are produced mainly by multiple-collision processes. The effect would be quite similar to the influence of electron capture on $2p\sigma$-vacancy production, examined in Appendices A and D of II. In Sec. III C we present evidence, though, which appears to indicate that multiple-collision processes do not play an im-

portant role in $3d\sigma$-vacancy formation. Hence, electron capture cannot be important in this formation either.

The second effect of electron capture is potentially more serious, because it could disturb the production of projectile x-rays *after* the $3d\sigma$-vacancy sharing between the collision partners has occurred (Sec. II). As shown in Ref. 35 and in Appendix B of II, the projectile x-ray cross section in a thick target is given by

$$\sigma_{\mathrm{proj}\,x} = F\omega\sigma^{p}, \tag{B1}$$

where

$$F = [1 + n v \tau(\sigma^{c} + \sigma^{p})]^{-1}. \tag{B2}$$

Here $\sigma^{p}$ is the vacancy production cross section, $\sigma^{c}$ is the electron capture cross section (including other possible quenching processes), $\omega$ is the fluorescence yield, $n$ is the target density and $\tau$ is the total radiative and Auger lifetime of the projectile vacancy. In solid targets it is difficult to evaluate $\tau$ because of uncertainties about the state of projectile ionization.[34] Also, the evaluation of $\sigma^{c}$ is uncertain, because even the recently refined electron-capture theory for slow collision[37] loses its validity if $Z_1/Z_2 \gtrsim 0.3$. Nevertheless, we present two evaluations of the factor $F$ which indicate that $F$ must be very close to unity in the cases of interest here: $L$ x-ray emission from 47–62-MeV I projectiles traversing solid targets with $Z_2 = 13$–40, and $K$ x-ray emission from 45–110-MeV Ni and Br projectiles traversing solid targets with $Z_2 = 50$–90.

First, following Ref. 38, we assume that for $\sigma^{c}$ one can use the Brinkman-Kramers[39] (BK) cross section, modified by Nikolaev[40] and scaled by a constant factor of 0.1. Guffy[41] has shown that such a scaling factor brings the BK electron-capture cross section into approximate agreement with experiment. Using single-vacancy values for vacancy lifetime $\tau$ (calculated from the radiative lifetime[21] and fluorescence yield[13]), we then compute $F$. Figure 13(a) shows $\sigma_{\mathrm{proj}\,x}$ for $L$ x rays from 47-MeV I projectiles traversing various solid targets. Figure 13(b) gives $F$. The same level-matching effects which enhance $\sigma^{p}$ give sharp decreases to $F$. Hence, if $F$ is correctly evaluated, one would expect to see dips in $\sigma_{\mathrm{proj}\,x}$ at the level-matching values of $Z_2$, similar to those seen in Ref. 36. The absence of the dips in $\sigma_{\mathrm{proj}\,x}$ is an indication that the calculated values of $\sigma^{c}$ are much too high (e.g., for 47-MeV I + Ti, $1.44 \times 10^{7}$ b) and that $F$ is actually close to unity.

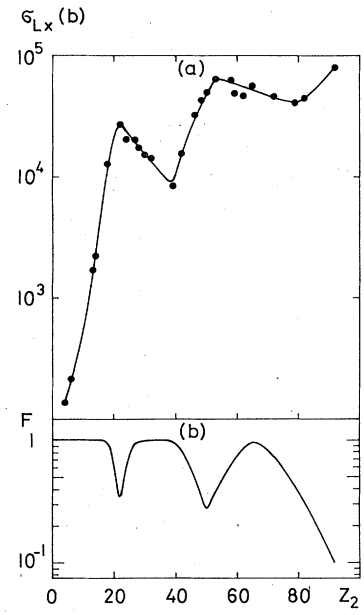


FIG. 13. (a) Total $L$-x-ray cross sections for 47-MeV $_{53}$I projectiles. Data from our work. (b) Expected attenuation factor $F$ [Eq. (B2)] for the observed cross section, if capture cross section is computed by scaled Brinkmann-Kramers formula. See Appendix B for details.

A second possibility, also used in Ref. 38, is to estimate $\sigma^{c}$ by the Demkov model.[20] In this model, which is based on a molecular-orbital approach, the cross section is equal to the product of a geometrical cross section $\pi a^2$ and the probability that a vacancy is transferred from the projectile to the target. At the level matching point the latter probability has its maximum value of the order of unity. Therefore, according to this model $\sigma^{c} \lesssim \pi a^2$, where $a$ should be close to the larger of the matching shell radii. For capture of Ti $K$ electrons into the I $L$ shell $\pi a^2 \simeq 2 \times 10^5$ b. This is two orders of magnitude smaller than the scaled BK cross section and gives a value for $F$ very close to unity. Similarly, one finds for the $K$-x-ray emission cross section from 45–110-MeV Ni and Br projectiles that $F$ is very close to unity (see also Sec. II B 3 in II). We conclude, that in the slow collisions of interest here, electron capture does not play an important role, as already suggested by Bell.[36]

---

†Permanent address: Hahn-Meitner Institut für Kernforschung Berlin, Bereich Kern-und-Strahlenphysik, and Freie Universität Berlin, Fachbereich Physik, D-1000 Berlin 39, West Germany.

[1]W. E. Meyerhof, R. Anholt, T. K. Saylor, S. M. Lazarus, A. Little, and L. F. Chase, Jr., Phys. Rev. A 14, 1653 (1976) (Paper I).
[2]W. E. Meyerhof, R. Anholt, and T. K. Saylor, Phys.

Rev. A 16, 169 (1977) (Paper II).
[3]R. Anholt and W. E. Meyerhof, Phys. Rev. A 16, 190 (1977) (Paper III).
[4]M. Barat and W. Lichten, Phys. Rev. A 6, 211 (1972). References to prior experiments on $K$-$L$ level matching can be found here.
[5]W. R. Thorson, Phys. Rev. A 12, 1365 (1975).
[6]W. E. Meyerhof, Phys. Rev. Lett. 31, 1341 (1973).
[7]F. C. Jundt, H. Kubo, and K. H. Purser, in *Proceedings of the International Conference on Inner-Shell Ionization Phenomena and Future Applications, Oak Ridge, 1973*, edited by R. W. Fink *et al.* (U.S. ERDA, Oak Ridge, 1973), p. 1450.
[8]H. Kubo, F. C. Jundt, and K. H. Purser, Phys. Rev. Lett. 31, 674 (1973).
[9]H. Kubo, Ph.D. thesis (University of Rochester, 1973) (unpublished); F. C. Jundt (private communication).
[10]S. Datz, C. D. Moak, B. R. Appleton, M. D. Brown, and T. A. Carlson in *Electronic and Atomic Collisions*, edited by L. M. Branscomb *et al.* (North-Holland, Amsterdam, 1971), p. 409; S. Datz, C. D. Moak, B. R. Appleton, and T. A. Carlson, Phys. Rev. Lett. 27, 363 (1971).
[11](a) S. Hagmann, Ph.D. thesis (University of Cologne, Germany, 1977) (unpublished); (b) S. Hagmann, P. Armbruster, and P. H. Mokler, *Abstracts of the Tenth International Conference on the Physics of Electronic and Atomic Collisions*, edited by M. Barat and J. Reinhardt (Commisariat à l'Energie Atomique Paris, 1977), p. 898.
[12]Further references are listed in Papers I and II.
[13]W. Bambynek, B. Crasemann, R. W. Fink, H. U. Freund, H. Mark, C. D. Swift, R. E. Price, and P. V. Rao, Rev. Mod. Phys. 44, 716 (1972).
[14]J. Eichler, U. Wille, B. Fastrup, and K. Taulbjerg, Phys. Rev. A 14, 707 (1976).
[15]N. Stolterfoht, D. Schneider, and D. Brandt, in Ref. 11(b), p. 902.
[16]P. Armbruster, P. H. Mokler, and H. J. Stein, in Ref. 7, p. 396.
[17]C. Foster, T. P. Hoogkamer, P. Woerlee, and F. W. Saris, J. Phys. B 9, 1943 (1976).
[18]E. E. Nikitin, Opt. Spektrosk. (USSR) 13, 761 (1962) [Opt. Spectrosc. (USSR) 13, 431 (1962)]; E. E. Nikitin, Adv. Quantum Chem. 5, 135 (1970).
[19]E. G. Bøving, J. Phys. B 10, L63 (1977).
[20]Yu. N. Demkov, Zh. Eksp. Teor. Fiz. 45, 195 (1963) [Sov. Phys. JETP 18, 138 (1964)].
[21]J. H. Scofield, At. Data Nucl. Data Tables 14, 121 (1974).
[22]There is some evidence that the parameters $\theta_k$ may vary with the energy difference $I_0$-$I_k$ in a regular manner. E. M. Middlesworth, Ph.D. thesis (University of Arizona, 1977) (unpublished); E. M. Middlesworth, Jr., D. J. Donahue, L. C. McIntyre, Jr., and E. M. Bernstein, Phys. Rev. A (to be published).
[23]J. A. Tanis, Ph.D. thesis (New York University, 1976) (unpublished); J. A. Tanis, B. Budick, J. W. Kast, and A. M. Rushton (unpublished).
[24]K. Helfrich and H. Hartmann, Theor. Chim. Acta (Berlin) 16, 263 (1970).
[25]W. E. Meyerhof, in *Abstracts of the Second International Conference on Inner-Shell Ionization Phenomena*, edited by W. Mehlhorn (University of Freiburg, Germany, 1976), p. 62; and in *Abstracts of the Fifth International Conference on Atomic Physics*, edited by R. Marrus, M. H. Prior, and H. A. Shugart (University of California, Berkeley, 1976), p. 64.
[26]B. Fastrup, in *The Physics of Electronic and Atomic Collisions*, edited by J. S. Risley and R. Geballe (University of Washington, Seattle, 1975), p. 361.
[27]J. S. Hansen, Phys. Rev. A 8, 822 (1973).
[28]K. Taulbjerg and J. S. Briggs, J. Phys. B 8, 1895 (1975); J. S. Briggs and K. Taulbjerg, J. Phys. B 8, 1909 (1975); Corrigendum, J. Phys. B 9, 1641 (1976).
[29]D. H. Madison and E. Merzbacher, in *Atomic Inner-Shell Processes*, edited by B. Crasemann (Academic, New York, 1975), Vol. I, p. 1.
[30]W. Brandt, in Ref. 7, p. 948.
[31]T. J. Gray, G. M. Light, R. K. Gardner, and F. D. McDaniel, Phys. Rev. A 12, 2393 (1975).
[32]T. J. Gray, *Proceedings of the Third Conference on Applications of Small Accelerators*, USAEC-CONF-741040-P1 (U.S. ERDA, Office of Public Affairs ) (National Technical Information Service, U. S. Dept. of Commerce, Springfield, Va., 1975), Vol. 1, p. 436.
[33]G. H. Pepper, R. D. Lear, T. J. Gray, R. P. Chaturvedi, and C. F. Moore, Phys. Rev. A 12, 1237 (1975).
[34]S. Data, Nucl. Instrum. Methods 132, 7 (1976).
[35]H.-D. Betz, F. Bell, H. Panke, G. Kalkoffen, M. Welz, and D. Evers, Phys. Rev. Lett. 33, 807 (1974).
[36]F. Bell and H.-D. Betz, J. Phys. B 10, 483 (1977).
[37]G. Lapicki and W. Losonsky, Phys. Rev. A 15, 896 (1977).
[38]C. L. Cocke, S. L. Varghese, and B. Curnutte, Phys. Rev. A 15, 874 (1977).
[39]H. C. Brinkman and H. A. Kramers, Proc. Acad. Sci. (Amsterdam) 33, 973 (1930).
[40]V. S. Nikolaev, Zh. Eksp. Teor. Fiz. 51, 1263 (1966) [Sov. Phys. JETP 24, 847 (1967)].
[41]J. A. Guffy, M.Sc. thesis (Kansas State University, 1974) (unpublished).